Pergamon

0734-743X(95)00003-8

Int. J. Impact Engng Vol. 16, No. 3, pp. 479–498, 1995

0734-743X/95 $9.50 + 0.00

YAWING IMPACT ON THIN PLATES BY BLUNT PROJECTILES

WERNER GOLDSMITH, ERIC TAM† and DAVID TOMER‡

Department of Mechanical Engineering, University of California, Berkeley, CA 94820, U.S.A.

(*Received* 19 *November* 1993; *in revised form* 25 *August* 1994)

Summary—Two experimental investigations and a corresponding analytical study were conducted to examine the phenomena attendant to the impact of blunt-nosed, hard-steel strikers on stationary thin plates of aluminum and steel at moderate angles of yaw and zero obliquity. The variation of ballistic limit with yaw angle or the terminal velocity and final trajectory angle in perforation tests were ascertained. Post-mortem examination of the plates indicated that damage and failure occurred by bulging, lateral indentation, and side and front petaling. A theoretical model based on a membrane representation was developed that analyzed the impact by dividing the process into five stages. This model underpredicted the ballistic limit by up to 14%, with better correlation found at higher yaw angles. Excellent agreement was observed between the experimental and analytical final velocities when the data points were corrected to reflect the difference between the experimental values of the ballistic limit and that predicted by the model. Fair agreement was found between the experimental and the analytical values of the trajectory angle.

NOTATION

a	projectile radius
b'	$d \tan \alpha$
c	wave velocity
d	projectile diameter
h	target thickness
h'	thickness of plug still attached to plate
m	mass
r	radial coordinate, radius
r_2	moment arm of shear force
t	time
v	velocity
w	transverse target displacement
x, y	coordinates, coordinate directions
x'	direction rotated by angle Φ counterclockwise from x
F	force
I	moment of inertia
L	projectile length
M	moment
P	force acting after conclusion of shearing
S	yield stress
U	work done by stresses acting on striker face
V	embedded volume
Z	percent increase in ballistic limit with yaw
α	yaw angle (angle between velocity vector and projectile axis)
β	oblique angle (angle between the target normal and the velocity vector)
δ	plate deflection in the normal direction
ε	strain
θ	circumferential angle and direction
ρ	density
Φ	trajectory (or impact) angle: (angle between the target normal and the projectile axis: $\lvert\Phi\rvert = \lvert\alpha\rvert - \lvert\beta\rvert$)
σ	stress
ϕ	half-angle subtended by arc radius r of plug still attached to plate

† Current address: Oil Systems, San Leandro, CA, U.S.A.

‡ Current address: Rafael, P.O. Box 2250, Haifa, Israel.

Subscripts:

a	adjusted
d	drag
dyn	dynamic
e	effective
f	final
ℓ	lift
0	initial
p	projectile
r, x, y, Θ	along corresponding coordinate directions
x′	along yawed projectile axis
sh	shear
t	target
th	theoretical
ult	ultimate
G	about mass centre G
P	along direction of P

INTRODUCTION

Projectile impact on stationary objects, including thin targets (where stress and deformation gradients throughout the thickness are neglected), has been investigated extensively, but most frequently for situations when obliquity, yaw and rotation of the striker are not present [e.g. 1–5]. Such idealized situations are never encountered in practice; however, their study greatly facilitates the assessment of collisions that involve one or more of these types of movements. Since the present inquiry is concerned with sub-ballistic impact of projectiles ($L/d < 5$), rather than long rods, work concerned with hypervelocity impact or kinetic energy penetrators, although extensive [e.g. 6], will not be generally reviewed here.

A number of theoretical and experimental investigations have been reported for other types of collisions, particularly for oblique impact [e.g. 7–13]. Backman and co-workers [2,12,13] depicted this phenomenon in terms of a phase diagram whose axes represented initial velocity and obliquity. The event consisted of regions of ricochet, embedment and perforation, with the striker either remaining intact or fractured. The predictions for exit speed and angle of a spherical striker were in excellent accord with corresponding measurement. The impact of spinning projectiles has also been examined [14,15]. While important, neither of these two topics bear directly on the present study.

Previous research of yawing strikers have been confined to long rods, where analytical and computer code results were compared with photographic and flash X-ray data [16–25]; these inquiries are also not intimately related to the current work. Bending waves have been examined extensively; in one study, where reverse ballistic techniques were employed [16], the depth of penetration produced was found to depend on both the rod diameter and the yaw angle.

Collisions with moving targets, which embody some of the features important for the collision of yawed strikers, have been described by Wu and Goldsmith [26,27] using a series of continuum representations. These model predictions, as well as those of a computer simulation [28], were found to be in reasonable agreement with corresponding experimental results. A technique for repeatable production of tumbling motion, its analytical modelling, and a preliminary set of target response has been described by Ruiz and Goldsmith [29]; a model for tumbling of long rods generated by oblique impact was proposed by Persechino and Williams [30].

This study is concerned with the penetration and perforation response of thin metallic plates in the vertical plane due to modest yaw impact, up to 19°, of small caliber projectiles fired with zero initial obliquity at subordnance speeds. Strikers with diameters of 6.35 mm and aspect ratios of 3 impinged on aluminum and steel at speeds of the order of 10–200 m/s. The predictions of an analytical model for this process are compared with the experimental results.

EXPERIMENTAL ARRANGEMENT AND PROCEDURE

The general arrangement for the tests has been previously described in substantial detail [26,31]; a schematic of the system is presented in Fig. 1. The propulsion mechanism for the principal tests consisted of a pneumatic gun, supported on a heavy table, with two interchangeable barrels of 12.7 mm and 6.35 mm diameter; the former was used for the yaw tests which required a sabot, while the latter was used for some shots at normal incidence that did not require a holder. Projectile speed was determined from signals produced by the interruption of two parallel laser beams directed across its trajectory. The gun can launch a 6.7 g projectile/sabot combination at a peak speed of about 250 m/s. However, in one of the test sequences, the projectiles were fired by means of a powder gun capable of producing speeds up to 2000 m/s.

Two series of blunt-nosed cylindrical projectiles were fabricated from oil-hardened drill rod. The first series utilized strikers of 6.2 mm diameter, 19 mm length, masses of 4.5 g with a hardness R_C 50; for a second sequence, these values were 6.35 mm, 20 mm, 5 g and R_C 60. These cylinders did not deform in any of the tests, justifying their representation as a rigid body in the subsequent analytical development.

In order to generate impact at the desired angle of yaw, the projectiles were initially embedded in a sabot with length, diameter and mass of 19 mm, 12 mm and 2.2 g for the first series and 12.7 mm length and diameter with a mass of 2.9 g for the second. The smaller sabot was made of polycarbonate, slotted so as to fly apart upon impact, while the second involved an integral Teflon cylinder. Holes with diameters corresponding to those of the projectiles, with a slight interference fit that ensured their union during flight were drilled into the sabots at obliquities of 0, 5, 10, 15 (and, for the second series, 19) degrees. Small yaw angles correspond to those found in practice and are, furthermore, required for trajectory stability. Hole depths ranged from 9.5 to 10.2 mm. Extensive attempts to remove the sabots from the projectile prior to target contact by impingement on sabot strippers failed; while separation was effected, the strikers were subjected to an undesired tumbling motion. In consequence, the striker/sabot combination invariably struck the target, but the sabot was removed almost immediately after initial contact. Post-mortem examination of the targets revealed only an annular superficial mark on the entry side, attributable to

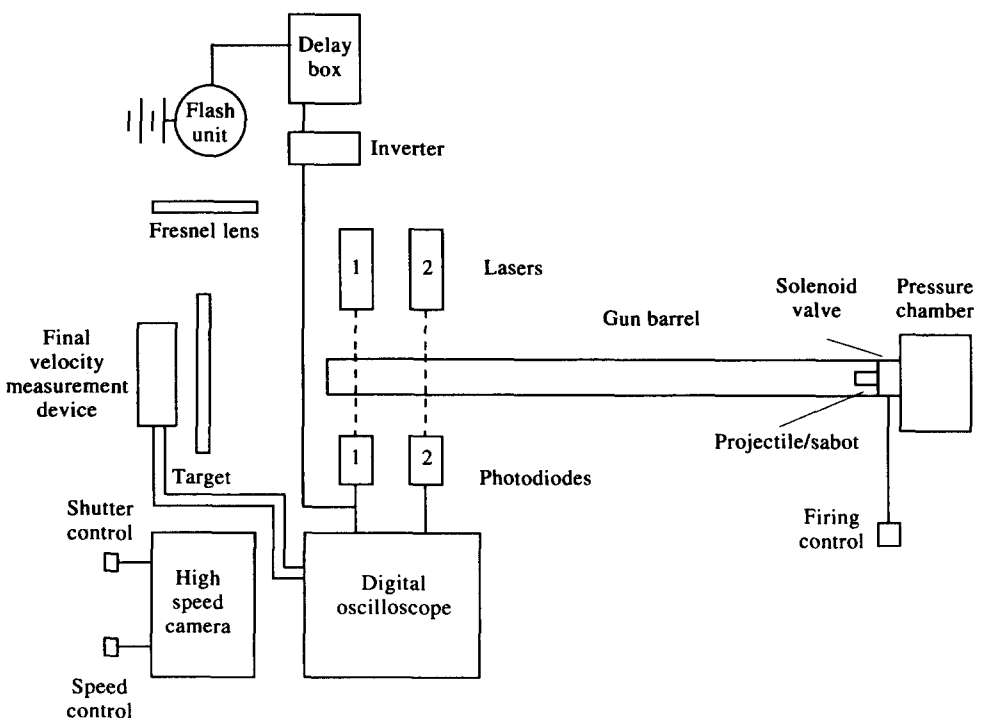

Fig. 1. Schematic of experimental arrangement.

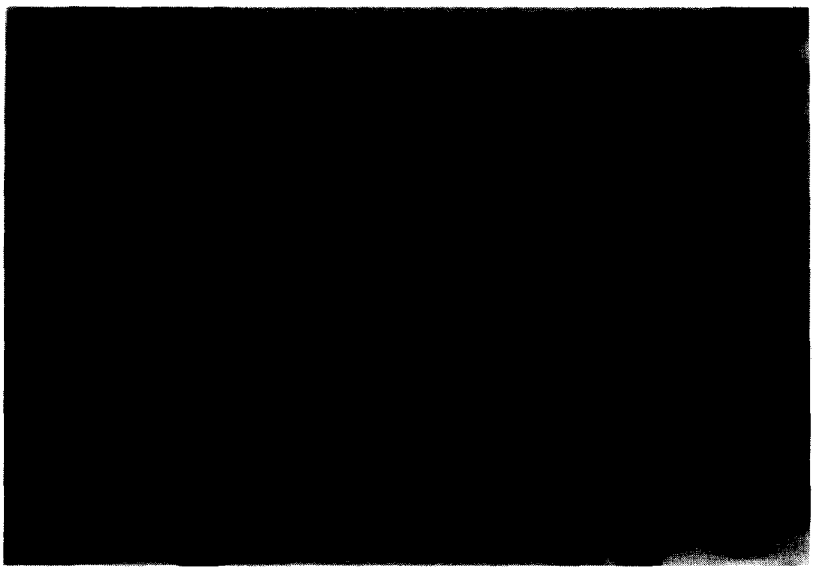

Fig. 2. Exit side view of target in holder.

the impact of the sabot, with no observable indentation. In consequence, and since this contact immediately removed the sabot, its presence was not considered to affect the perforation mechanisms, although the effective mass of the striker during initial penetration might require some adjustment.

Targets consisted of 140 mm diameter circular plates of 2024-0 (fully annealed) aluminum with a thickness of 3.175 mm or SAE 4130 steel with thicknesses of either 1.59 mm or 3.175 mm. The yield and ultimate tensile strength and tensile failure strain of the completely annealed aluminum series were selected as 200 MPa, 240 MPa and 0.22 (taken from [26]).† For the SAE 4130 steel whose hardness was measured to be R_C 22, the corresponding values for the first series were selected as 560 MPa, 780 MPa, and 0.28, while the yield and failure stresses for the second series (with an R_C 30) were found to be 690 and 930 MPa†, respectively. The targets were clamped inside two circular brackets and a corresponding steel holder that was bolted to the table, as shown in Fig. 2. Side constraints were removed to permit high-speed photographic examination of the perforation process. On the average, the distance of the target from the muzzle of the gun was 190 mm.

In a number of tests, the exit velocity of the striker was determined from the signals generated by the closure of an electric circuit for each of two sets of closely spaced parallel aluminum foils held in wooden frames; this eventuated after the metallic projectile produced contact between these sheets when they ruptured. In other experiments, this velocity as well as the perforation event were obtained from a series of 79 individual frames recorded by a Beckman–Whitley W2 framing camera using 35 mm film and operating at speeds of 44,000–50,000 pictures per second, controlled by a rheostat [29]. Illumination by a Singer Graflex Strob 250 unit powered by a 512 V battery produced backlighting with a duration of 1.2 ms. Placement of a Fresnel lens in front of this unit provided a parallel light field for the camera. The signal from the first photodiode triggered a flash delayed so as to permit a view of the striker both before and after the impact.

The film provides the principal record of the phenomenological aspects of the perforation. Comparison of the initial velocity from these photographs with the measured value from laser beam interruption indicates a discrepancy of 4%, which, together with an estimated experimental inaccuracy of 1% amounts to a potential data error of 5%. The oblique angle determined from the film is only the component in the plane normal to the camera view;

† Strength magnitudes vary depending on heat treatment. Even treatments listed as identical have resulted in different quoted values in the literature.

the deviation from the actual angle is estimated from the screen rupture patterns to be about 10%. The permanent deflection of the target was measured by means of a mechanical comparator. Further details concerning the equipment and operation may be found in [26] and [29].

PERFORATION MODEL

A perforation model based on a number of simplifying assumptions has been developed to describe the present situation of yawing impact of a blunt, short rigid cylinder of mass m_p, length L and diameter d on a thin, metallic plate moving strictly in the vertical plane due to bilateral symmetry. The representation is partly based on a post-mortem examination of the test specimens and partially on analyses developed for other non-normal collisions [27]. Figure 3 depicts the geometry and nomenclature for impact on a thin target in the vertical plane, involving the yaw, oblique and trajectory angles α, β, and Φ. Yaw angle α is defined as the angle between the velocity vector of the striker and the projectile axis (oriented in direction x'), β is the angle between the normal to the target (located horizontally and assigned direction x here) and the velocity vector, and trajectory angle Φ is the angle from the target normal to the projectile axis, $\Phi=\alpha-|\beta|$. The y-axis is taken as the vertical. The counterclockwise direction is regarded as positive.

Projectile perforation with yaw is modelled here as a set of 5 separate stages, as portrayed in Fig. 4, after first contact (Fig. 4a): (1) initial penetration of the striker into the target without angular deviation or plate deflection under essentially quasi-static conditions, shown in Fig. 4b; (2) striker/plate interaction resulting in deformation and tensile failure of the target while the presence of yaw is neglected, depicted in Figs 4c and 4d; (3) an initial striker rotation produced by the non-symmetric stress distribution due to oblique entry, Fig. 4e; (4) additional angular changes while a plug is sheared from the target, Fig. 4f; and (5) petaling of the target caused by side contact with the striker, Fig. 4g, followed by its exit, Fig. 4h. Stages (2) and (3) are contemporaneous, while all others are successive; the analysis for stages (2) and (5) has been adapted from [27].

The striker motion during stage (1) is considered to be represented by pure translation until the entire face has made contact with the target. Due to its brief duration and the quasi-static nature of this stage, plate motion during this interval is neglected. It is assumed, further, that the only significant stresses, distributed uniformly, act on the projectile on its front face and are at the yield limit, with the effect of those on the periphery considered to be negligible. The work done by the projectile on the target, U, is obtained by integrating the dot product of these normal stresses and the velocity vector over the embedded surface during the time of indentation; this is given by

$$U=\int_0^t\int_{\text{surface}}\bar{\sigma}\cdot\bar{v}\,\mathrm{d}A\,\mathrm{d}t \tag{1}$$

$$=S_eV_p=S_e(\pi/8)\mathrm{d}^3\tan\alpha \tag{2}$$

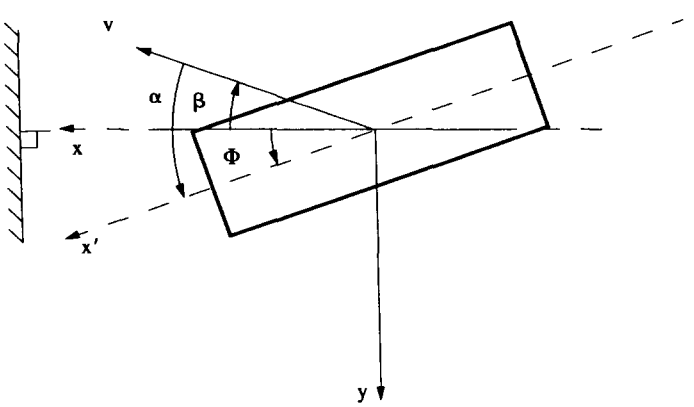

Fig. 3. Definition of the yaw angle, α, oblique angle, β, and trajectory angle, Φ.

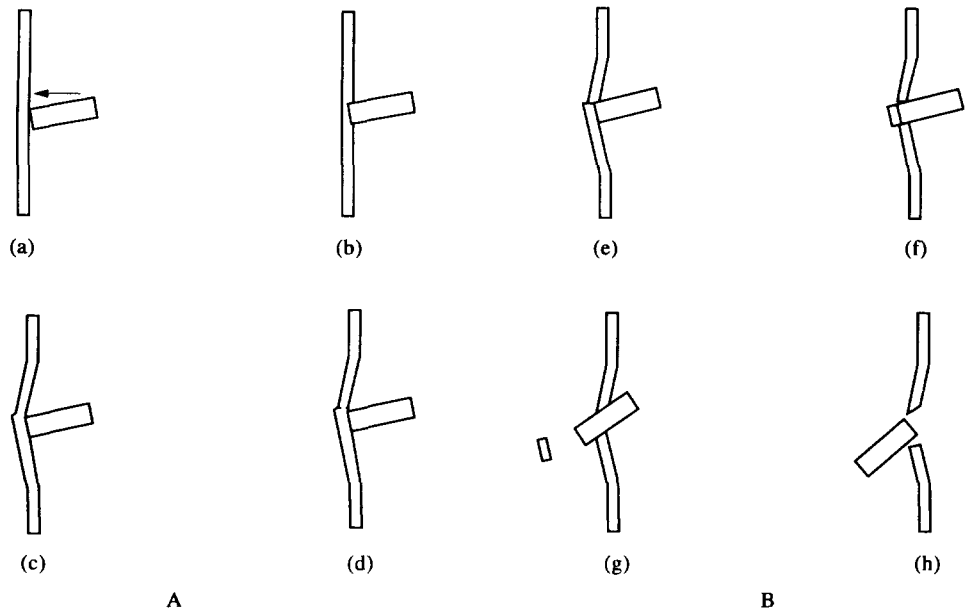

Fig. 4. (A): Penetration model for impact with yaw of a cylindrical projectile on a thin plate: (a) initial contact; (b) indentation; (c) initial projectile rotation; (d) tensile failure. (B): Perforation model for impact with yaw of a cylindrical projectile on a thin plate: (e) initial projectile rotation; (f) plug shearing; (g) plug ejection and petaling; (h) exit of the projectile.

if the velocity vector is taken parallel to the x-direction (Fig. 3). Here, S_e is the effective yield stress and V_p the embedded projectile volume for this stage. For the present experimental conditions, the striker indentation is less than the target thickness so that stage (1) does not result in plate failure. In view of the high loading rate, the yield stress S is taken at its dynamic value S_{dyn}; further, it is multiplied by the factor 1.75 to account for the constraint to side flow in plates [31]. Thus, the effective yield stress S_e is given by

$$S_e = 1.75 S_{dyn}. \tag{3}$$

The work–energy equation then provides the velocity v_1 at the end of this interval as

$$v_1 = [v_0^2 - (2U/m_p)]^{1/2}. \tag{4}$$

After stage (1), the interaction will be modelled as normal impact on a stationary target in view of the small oblique angles encountered in the experiments and a velocity vector that is normal to the plate. A membrane model [32] for very thin plates with ratios of thickness to projectile radius $(h/a) < 1$ was found to portray the impact process very well; the documentation and details of the analysis are given in [27]. This representation will also be employed for the present situation where $(h/a) = 1$. The validity of such a model was supported by the observed tensile failures at the upper crater edge in the targets whose presence also obviate the need for a constraint factor for the dynamic yield stress which is regarded as constant. Rigid/perfectly-plastic behaviour of the plate and a rigid striker are also assumed. The motions of both the target plate and the projectile are axisymmetric in view of the circular cylindrical projectile shape and the direction of its velocity vector.

Penetration entails plastic wave propagation, common motion of the striker and target when the wave reaches the distal face, and tensile failure of the plate. From conservation of linear momentum, the velocity of the interface of the incipient plug, v_2, for a completely inelastic impact is given by

$$v_2 = m_p v_1 / (m_p + \rho_t \pi h a^2) \tag{5}$$

where ρ_t is the target density. The plate kinematics and the corresponding radial strain, $\varepsilon_{rr} \approx \frac{1}{2}\left(\frac{\partial w}{\partial r}\right)^2$ are evaluated using a finite-difference solution of the axisymmetric form of the wave equation for the region of the plate governed by plastic shear [27,32], which propagates with speed $c_{sh} = (S/\rho_t)^{\frac{1}{2}}$, and by the projectile interface; radial motion is neglected. The initial conditions are given by Eqn (5), zero displacement at $r = a$, and zero velocity for $r > a$.

For completely normal impact, tensile failure first occurs when the radial strain ε_{rr} in its mid-plane at the periphery of the striker attains the ultimate tensile strain of the material. Because of axial symmetry, this fracture is complete and results in ejection of a plug. The projectile subsequently encounters no further resistance.

However, for yaw impact, it was found experimentally that, due to the inclination of the striker, only the upper portion of the plate was pierced as the result of tensile (membrane) forces. Thus tensile failure is a necessary, but not a sufficient condition for target perforation. The second condition for perforation is developed during stage (4). Projectile rotation, concurrent with indentation in stage (3) and defined by angle β, will now be examined.

At the end of indentation, two normal stress components σ_{rr}, $\sigma_{x'x'}$ and shear stress $\sigma_{r\theta}$ act on the striker surface in contact with the target in the axial, radial and circumferential direction, respectively, as shown in Fig. 5; these are postulated to have attained the dynamic yield value S_{dyn}, based on the results found for 2024-0 aluminum in [33]. Only the first two stress components result in a moment about the mass center G of the striker; the third does not due to bilateral symmetry. Integration yields the moment due to σ_{rr} as

$$M_{rr} = Sdb'(L - b')/\pi \tag{6}$$

where $b' = d \tan \alpha$ is the greatest contact distance along the surface of the projectile [34]. Similarly, the moment due to $\sigma_{x'x'}$ is

$$M_{x'x'} = Sd^2b'/\pi. \tag{7}$$

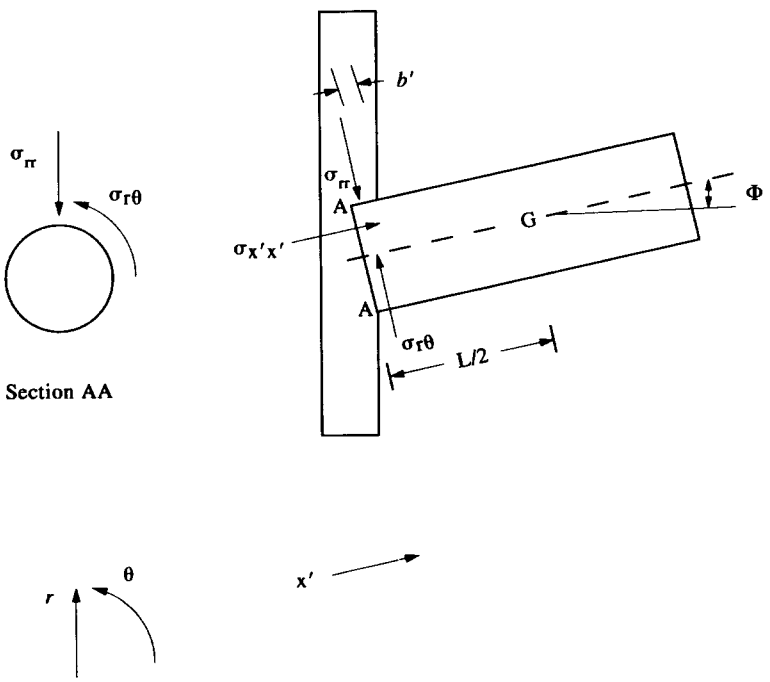

Fig. 5. Stresses acting on yawed, embedded projectile.

These moments act in opposite directions. The net moment, $M_G = M_{rr} - M_{x'x'}$ produces an angular acceleration $\ddot{\Phi}$ which, for a small time interval Δt, can be approximated by

$$M_G = I_G(\Delta\dot{\Phi}/\Delta t) \text{ with } I_G = (1/4)m_p a^2 + (1/12)m_p L^2 \tag{8}$$

where I_G is the moment of inertia about the mass centre.

For the short plugging times encountered, about 30 μs, it is reasonable to assume a constant (average) velocity

$$\dot{\Phi} = M_G t_2/I_G \text{ or the change in the trajectory angle } \Delta\Phi = \dot{\Phi} t_2. \tag{9}$$

The value of t_2, measured as starting at the end of stage (1), is either the time required for the generation of tensile failure or that needed for the plate to stop the projectile.

After initial tensile failure of the plate, the striker does not encounter further resistance from the upper plug/plate interface. Experiments indicate that, at the onset of failure, this region constitutes an arc of about 90°. Thus, the force that opposes further motion of as well as the torque rotating the projectile arise from the shear stress at the periphery of the plug subtended by the remaining 270°. This shear force F_{sh} is then quasi-empirically given by

$$F_{sh} = (3/2)\pi d\, h'\langle t\rangle S \tag{10}$$

where $h'\langle t\rangle$ represents the continually diminishing thickness of the plug still attached to the plate. Its moment arm, in terms of the arc radius r subtended by an angle of 2ϕ, is $r(\sin\phi/\phi)$. The shear stress is taken as the value of the yield stress based on the results obtained by Liss *et al.* [33] for 2024-0 aluminum plates.

Application of the linear and angular impulse–momentum principle to the projectile during a time step Δt provides the change in linear and angular velocity during this interval as

$$v = (F_{sh}\Delta t)/m_p \qquad \text{and} \qquad \Delta\dot{\Phi} = (F_{sh} r_2 \Delta t)/I_G \tag{11}$$

where r_2, the moment arm of F_{sh}, is taken as constant. The values of the updated translational and rotational velocity and the new oblique angle are given by

$$v = v_0 - \Delta v \quad \text{(a)}; \qquad \dot{\Phi} = \dot{\Phi}_0 + \Delta\dot{\Phi} \quad \text{(b)}; \qquad \Phi = \Phi_0 + \dot{\Phi}\Delta t \quad \text{(c)} \tag{12}$$

where the new value of F_{sh} is obtained from Eqn (10).

The value of v_0 at the initiation of plug shear is the normal component of the velocity obtained using the membrane equations of motion for plate and projectile and the associated boundary conditions, i.e.

$$v_0 = \left[\frac{\partial w}{\partial t}\cos\beta\right]_{t=t_3} \tag{13}$$

where t_3 is the time at the end of stage (3) and equals t_2 in view of the concurrence of stages (2) and (3). For Eqns (12a) and (13), it is assumed that the projectile velocity vector is parallel to its axis during this time interval.

With the further assumption that the plug and projectile move as a unit, the decrease in contact area thickness between plug and target is

$$\Delta h'\langle t\rangle = v\Delta t \quad \text{so that} \quad h'\langle t\rangle = h'\langle t_0\rangle - \Delta h'\langle t\rangle \tag{14}$$

where $h'\langle t_0\rangle$ is the value at the end of the previous time step. The value of $h'\langle t\rangle$ at the start of stage (4) is assumed to be $h'\langle t\rangle|_{t=t_2} = h/[\cos\Phi]|_{t=t_2}$; this stage ends when $h'\langle t\rangle$ reaches zero where the plug separates and no longer moves together with the striker, or else the projectile becomes embedded.

After the plug has sheared, contact of the upper striker periphery with the target creates a force P perpendicular to the axis, shown in Fig. 6, which produces deformation and elliptical hole enlargement of the plate as well as changes in the rigid-body motion of the projectile. The product of this force and the component of projectile velocity along its line of action, v_p, represents the power for stable crack expansion which initiates when the critical circumferential strain $\varepsilon_{\theta\theta}=\varepsilon_{ult}$ is attained. As shown in [27], this equality permits evaluation of P when the effects of friction are neglected. The change in the angular velocity of the projectile is then given by

$$\Delta\dot{\Phi}=(Pr_1\Delta t)/I_G \tag{15}$$

where r_1 is the distance from the line of action of P to the mass centre of the striker. The drag and lift force, P_d and P_l are the components of P along and perpendicular to $\mathbf{v}$ (resolved into v_x and v_y) and are given by

$$P_d=P\sin\alpha=P\sin(\Phi-\beta); \qquad P_\ell=P\cos\alpha=P\cos(\Phi-\beta) \tag{16}$$

where $\beta=\tan^{-1}(v_y/v_x)$. The drag force changes the striker speed by

$$\Delta v=(P_d\Delta t)/m_p \tag{17}$$

and the change in trajectory angle is

$$\Delta\Phi=(v\Delta t)/r_c \tag{18}$$

where r_c, the distance to the instant centre, is given by $r_c=(m_pv^2)/P_\ell$. The updated values of linear and rotational velocity, oblique and yaw angles can be determined by means of Eqns (9). During time interval Δt, the projectile position is given by

$$x=x_0+(v\cos\theta)\Delta t \qquad y=y_0+(v\sin\theta)\Delta t. \tag{19}$$

The impact ends when either the penetrator loses contact with the target after perforation, becomes embedded (or, equivalently, exits the plate with negligible velocity), or else ricochets. The first case occurs when $r_1>L/2$, while the latter ensues when the striker velocity is reduced to zero. Numerical results from this analysis were obtained using FORTRAN and a DEC VAX VS 3600 computer using the Ultrix operating system.

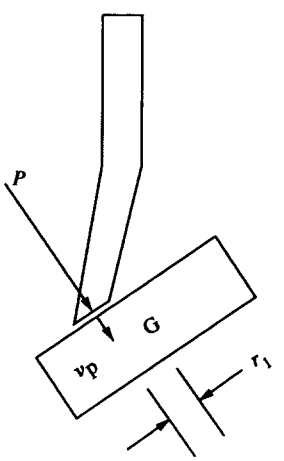

Fig. 6. Forces acting on yawing projectile during hole enlargement.

RESULTS AND DISCUSSION

(*a*) *Target damage*

A sequence of selected photographs portraying the perforation of a 3.175 mm thick 2024-0 aluminum plate by a projectile/sabot combination striking at an initial velocity of 193 m/s with a 15° angle of yaw is presented in Fig. 7; the series was taken at a camera speed of 44,320 frames per second and shows the splitting of the sabot. A simulation of the impact process below the ballistic limit is shown in Fig. 8; it depicts some features of the analytical model and consists sequentially of (a) penetration at the initial yaw angle, (b) further penetration due to rotation of the striker around point A that shears the target along the path of B without further penetration at A, and (c to e) subsequent further rotation around point C at the edge of the crater without an increase in the depth of penetration.

Selected results from the first series of tests, including the values of the peak plate deflection δ and of the ballistic limit v_{50} are summarized in Table 1 for the aluminum and steel targets. All plates experience bulging, especially in the vicinity of the contact area, as illustrated in Fig. 9 for the sub-ballistic-limit Run 16. This feature also occurred in the case of embedment, as shown in Fig. 10 for Run 36, and is almost entirely due to the membrane response of the target. For normal impact, bulging and plug ejection are the only damage mode due to axial symmetry.

Under conditions of yaw, the obliquity of the striker generates lateral indentation, as shown in the impact side in Fig. 11, Run 27; it results in an elliptic crater that is more pronounced for higher yaw angles. The photograph also indicates the absence of any

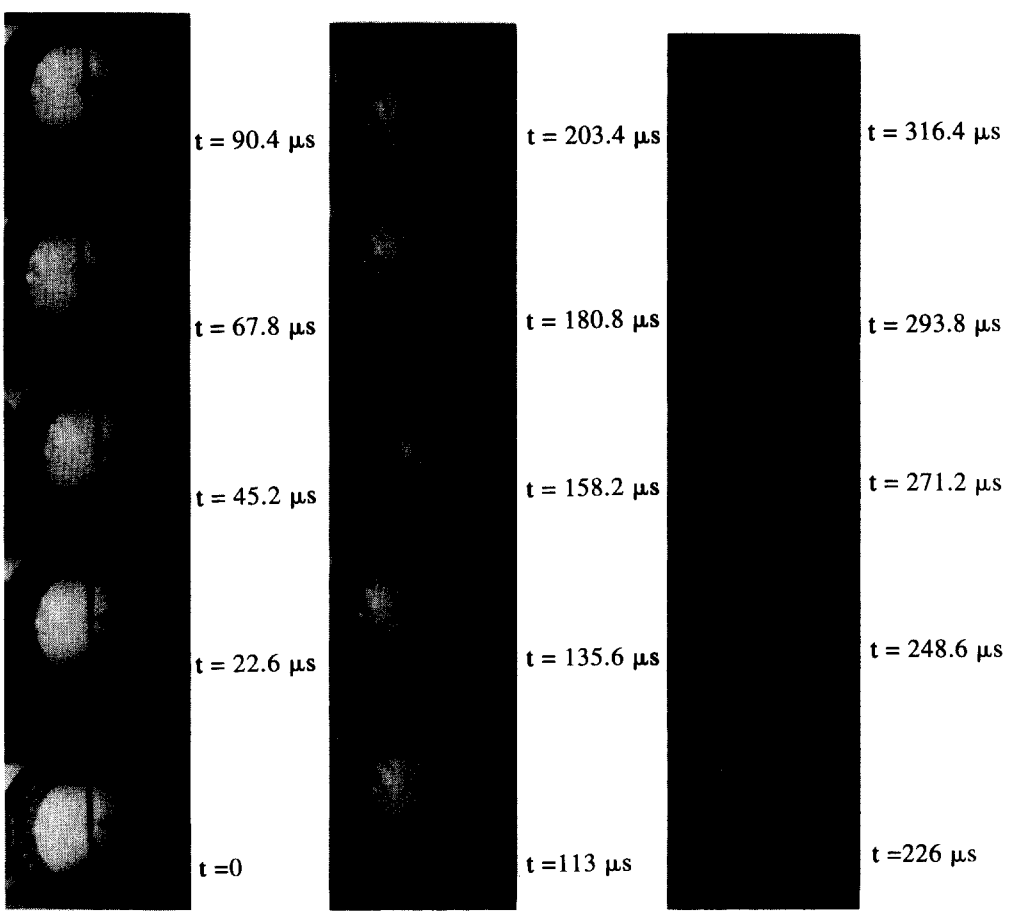

Fig. 7. Perforation sequence for Run 30, 2024-0 aluminum target struck at 193 m/s at a 15° yaw angle with a camera speed of 44,320 frames/s. The sabot is seen to break into two pieces.

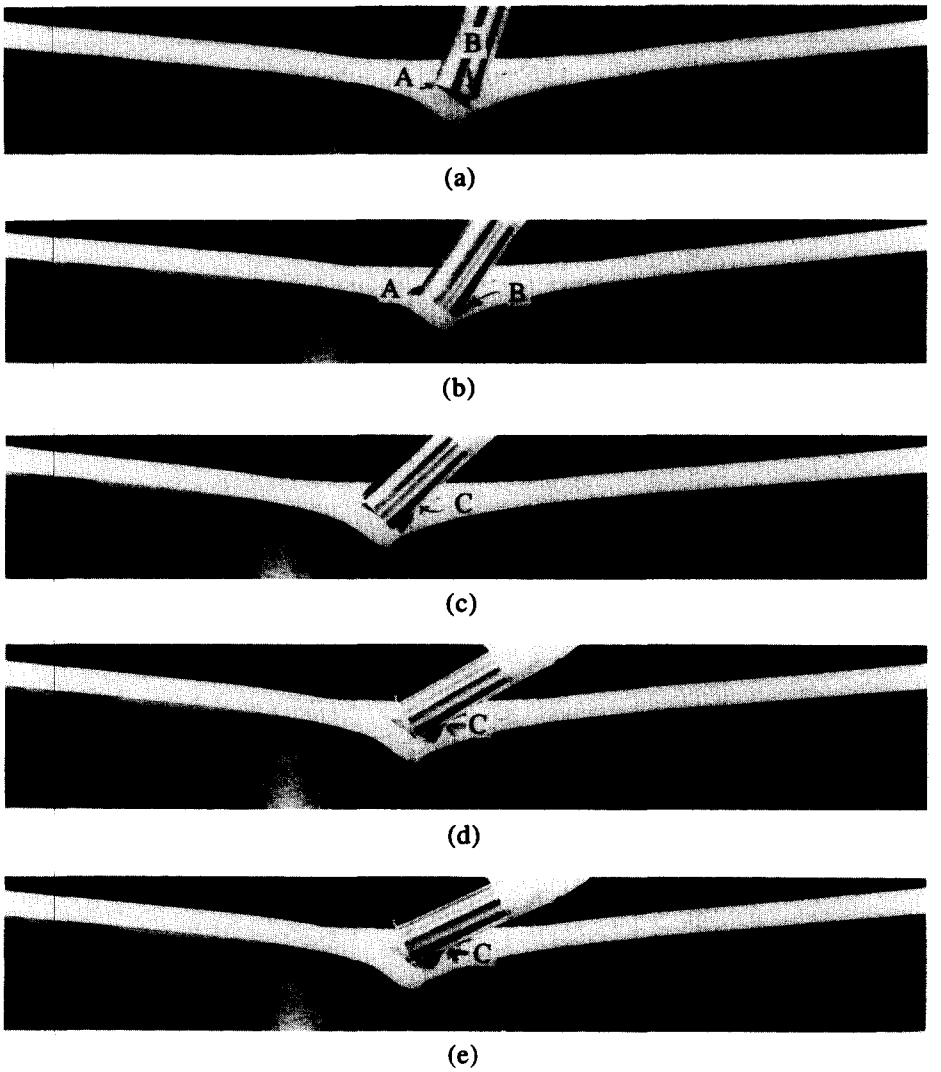

Fig. 8. Simulation of the penetration process: (a) initial penetration at initial yaw angle; (b) further penetration due to rotation of striker about point A and shearing of target occurring along the path of point B of the projectile without further indentation at A; (c)–(e) successive further rotation of striker around point C at the edge of the crater.

noticeable effect due to the presence of the sabot. On the other hand, normal impact generates a circular hole of final diameter slightly smaller than that of the striker due to elastic recovery.

Further plate damage occurs upon projectile perforation and subsequent dissociation from the plate with the generation of a larger hole on the exit side and cracks emanating from this discontinuity. Side petaling, where just one major crack is present, is manifested only at yaw angles of 10 and 15 degrees. Front petaling when two (or more) major cracks appear, as depicted in Fig. 12, occurs only at the highest yaw angle of this series. These features are very similar to the damage patterns observed in impact on moving targets [26,27]; however, the perforation imprint for the moving target consists of a triangular shank below a more or less circular apex, while that for yaw impact exhibits a more irregular pattern for the head and a shorter shank.

While normal penetration of the striker generates a symmetric plug by shearing, the oblique entry due to yaw, illustrated in Fig. 13 for Run 24, shows that plug removal begins with target failure along the upper edge of the contact area, the region of furthest penetration, while the plug is still in contact with the lower edge. Cross sections of perforated targets at increasing angles of yaw, but similar impact speeds, are shown in Figs 14a–14c for

Table 1. Results for aluminum and steel targets, first series

Run no	*α, Yaw angle, (deg)*	*Initial velocity, v_0 (m/s)*	*Perforation status*	*Final velocity, v_f (m/s)*	*δ, Maximum deflection (mm)*	*Final yaw angle (deg)*	*Comments*
				2024 *Aluminum*			
1	0	116	No				Embedment
2	0	134	No		13.2		
3	0	147	No				Embedment
4	0	152	No		10.7		No sabot
5	0	156	Yes		11.8		v_{50}
6	0	169	Yes	27	10.6		No sabot
7	0	193	Yes		11.1		
8	5	131	No		13.1		
9	5	146	No		14.5		
10	5	151	No				Embedment
11	5	151	Yes		10.6		v_{50}
12	5	156	Yes	27	12.7		
13	5	166	Yes	67	11.4	13	
14	5	183	Yes	127	11.8	16	
15	5	197	Yes	152	11.5	9	
16	10	155	No		14.8		
17	10	159	Yes		14.7		v_{50}
18	10	168	Yes	40	14.1	15	
19	10	176	Yes	78	13.5	31	
20	10	182	Yes	94	13.7	29	
21	10	193	Yes	120	13.3	19	
22	15	99	No		9.8		
23	15	132	No		12.6		
24	15	148	No		15.3		
25	15	161	No		17.2		
26	15	165	Yes		12.0		v_{50}
27	15	170	Yes	37	14.1		
28	15	171	Yes	61	13.1		
29	15	183	Yes	81	13.5	35	
30	15	193	Yes	105	13.2	26	
31	15	197	Yes	118	14.1	30	
32	15	208	Yes	144	15.1	24	
33	15	234	Yes	187	15.1	21	
				4130 *Steel*			
34	0	151	No		9.9		
35	0	170	Yes		7.1		v_{50}
36	0	175	No				Embedment
37	0	178	No		10.0		
38	0	181	Yes		7.5		
39	10	158	No		7.4		
40	10	163	No		7.6		
41	10	175	Yes		8.0		v_{50}
42	10	189	Yes		7.9		
43	10	195	Yes	39	8.1	11	

Runs 6, 19 and 29, respectively. These photographs show that resistance to plug ejection results from the cohesion at the lower interface edge, since the lower part of the target bends with greater curvature than the upper portion. Cross sections of both the aluminum and steel targets, 3.125 mm thick, from the second series of tests are exhibited in Figs 15a and 15b. These samples were struck at the ballistic limit velocity for normal impact, 133 m/s for aluminum and 152 m/s for steel, respectively, and increasing angles of yaw. The evolution of the plug and other phenomena described above are also manifested in these photographs.

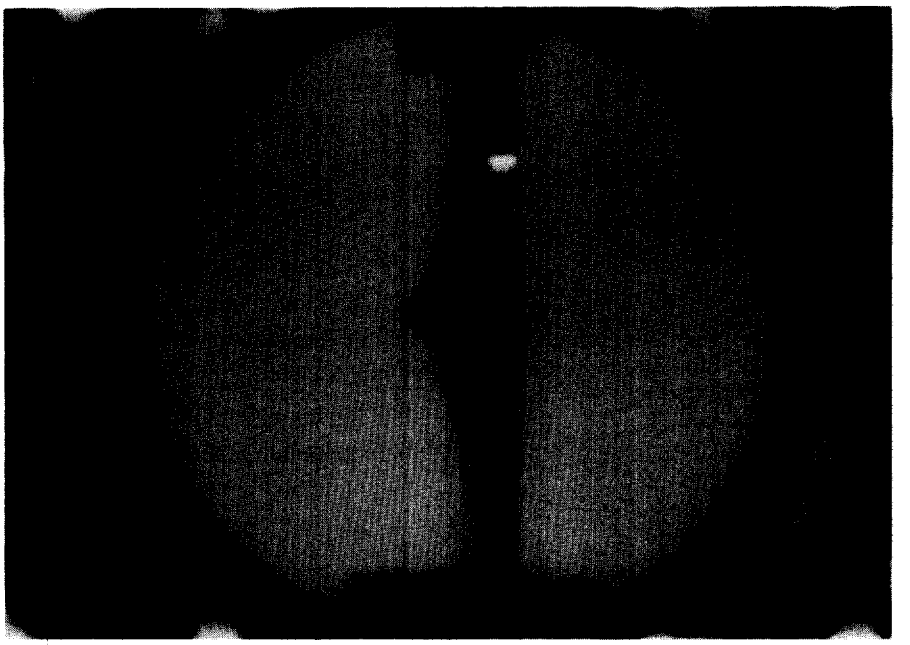

Fig. 9. Bulging of the aluminum plate for non-perforation Run 16 ($v_0 = 155$ m/s; $\alpha = 10°$).

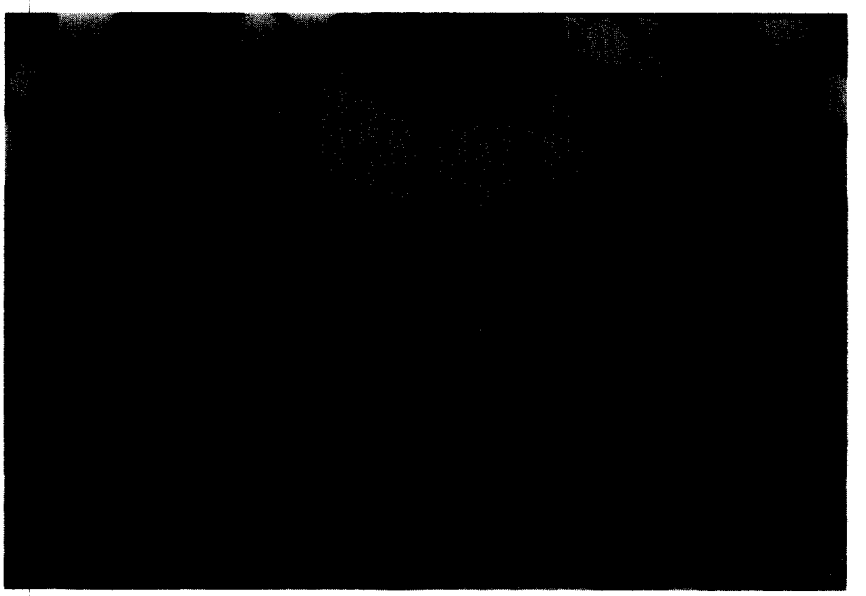

Fig. 10. Bulging of the steel plate at the ballistic limit, Run 36 ($v_0 = 175$ m/s, $\alpha = 0°$).

(*b*) *Ballistic limit*

The experimentally-determined ballistic limit velocities v_{50} for the 3.175 mm thick 2024-0 aluminum targets for series 1 and 2 are listed in the first portion of Table 2. Since this parameter represents the minimum average of a very large number of shots which just result in complete perforation, slight adjustments in the data were required to obtain this designated limit. This is due to slight variations in yaw angles and specimen material properties, and in view of the conduct of only a few tests for each impact condition. The data for series 2 were scaled to that of series 1 by the mass ratio of these tests, based on the hypothesis that initial momentum is the principal determinant for perforation. With

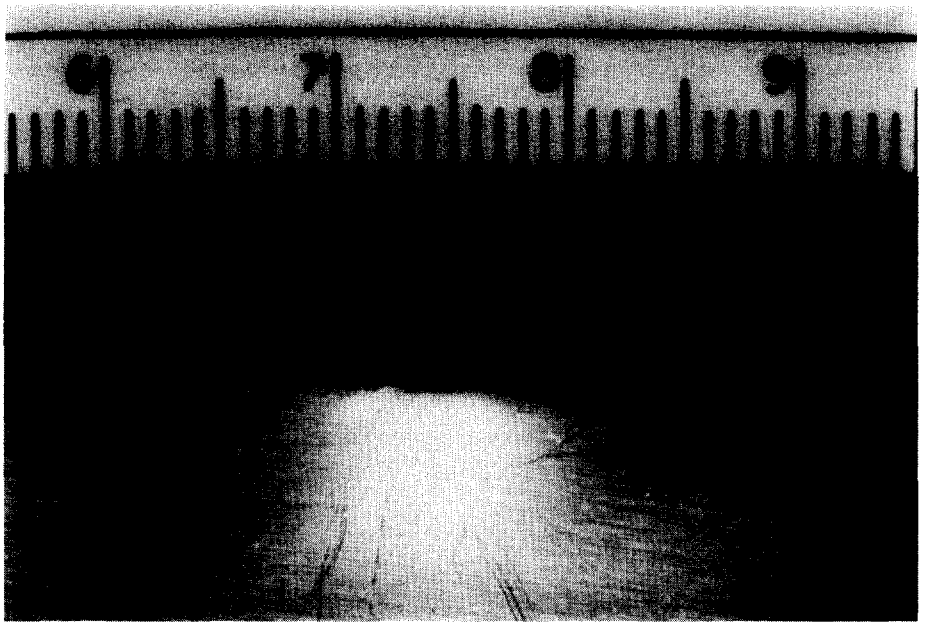

Fig. 11. Hole enlargement of the aluminum plate, Run 27 ($v_0 = 170$ m/s, $\alpha = 15°$).

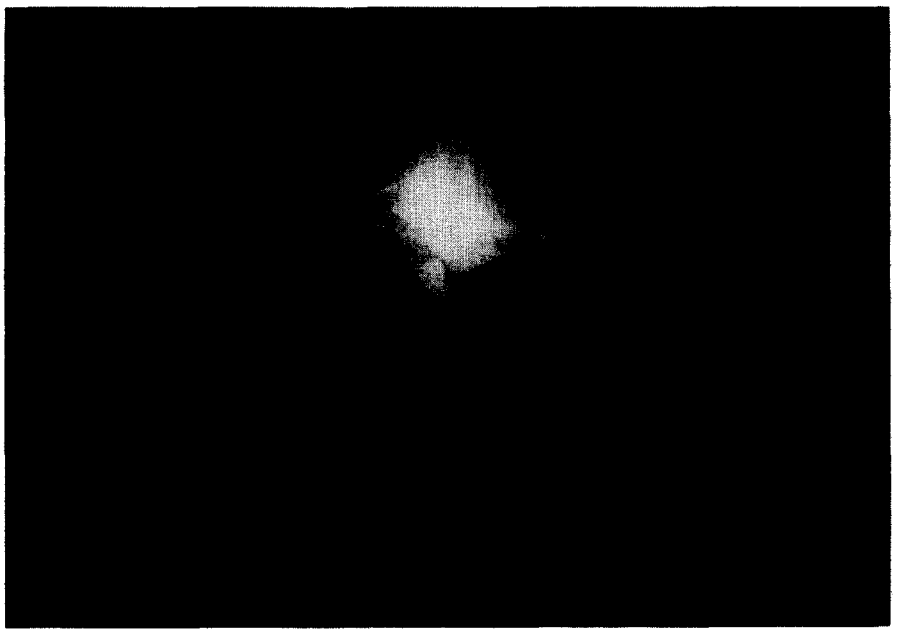

Fig. 12. Front petaling of the aluminum plate, Run 33 ($v_0 = 234$ m/s, $\alpha = 15°$).

this adjustment, the ballistic limit data correspond very well. It should also be noted that the sabots for series 2 consisted of hollow cylinders of polycarbonate that, unlike those for series 1, do not break into two pieces.

The theoretical value of the ballistic limit is critically affected by the choice of the dynamic yield strength which depends on the strain rate extant and the test arrangement. A comparison of the data from the series 1 aluminum tests with the predictions of the analysis is provided in the second section of Table 2; the computations have been performed on the basis of both a previously-employed yield strength S_y of 200 MPa [26] and for a value of 250 MPa. For the latter, the discrepancy is less than 5%.

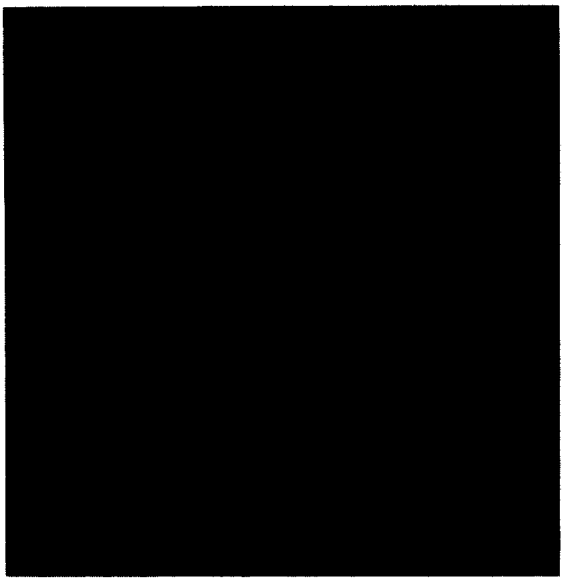

Fig. 13. Cross section of a nonperforated aluminum plate, Run 24 ($v_0 = 148$ m/s, $\alpha = 15°$).

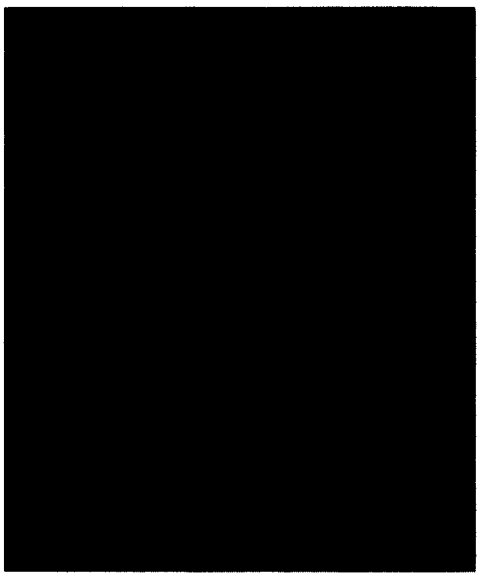

(a)

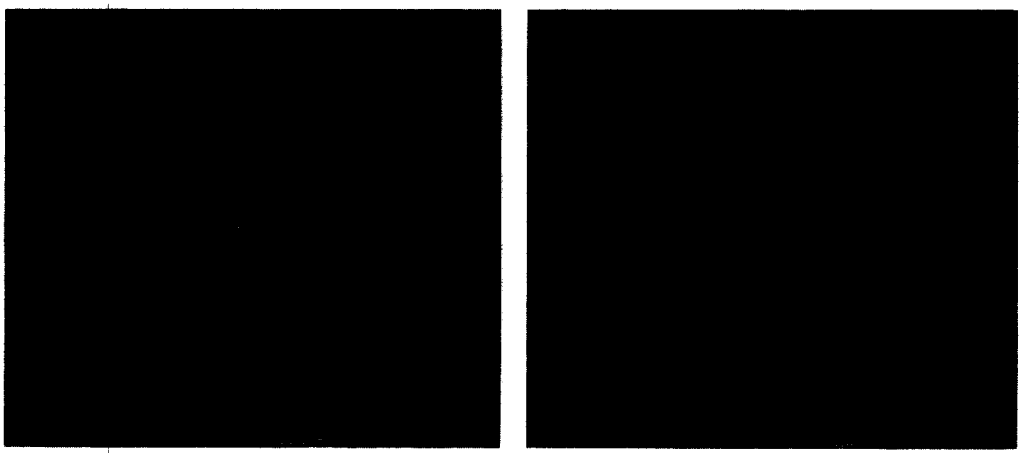

(b) (c)

Fig. 14. Cross section of aluminum plates for perforation runs: (a) Run 6 ($v_0 = 169$ m/s, $\alpha = 0°$); (b) Run 19 ($v_0 = 176$ m/s, $\alpha = 10°$), and (c) Run 29 ($v_0 = 183$ m/s, $\alpha = 15°$).

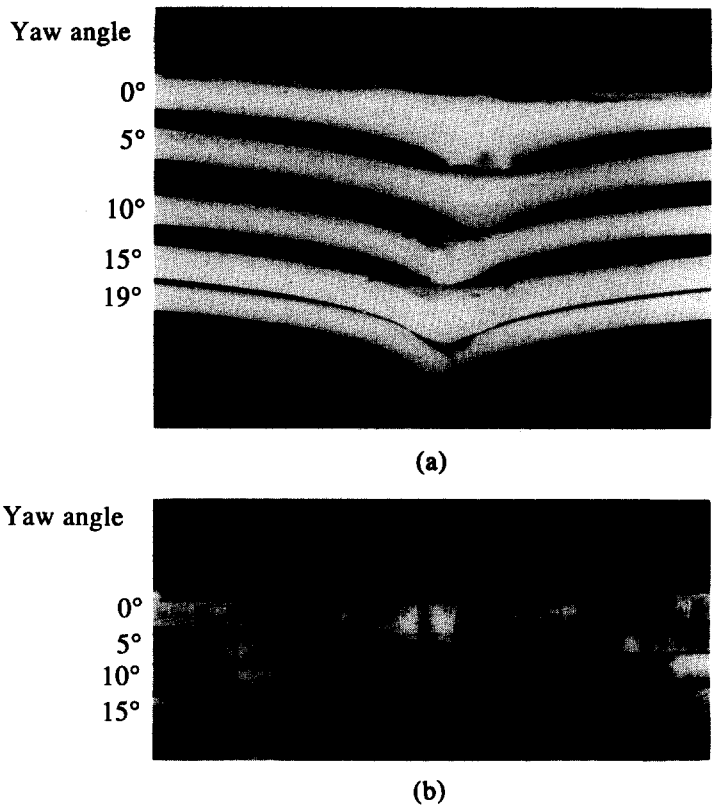

Fig. 15. Perforation into targets at the ballistic limit speed with yaw, Series 2: (a) Aluminum ($v_0 = 133$ m/s, $\alpha = 0°$, 5°, 10°, 15°, 19°); (b) Steel ($v_0 = 148$ m/s, $\alpha = 0°$, 5°, 10°, 15°).

It is noteworthy that the results obtained here are consistent with similar comparisons involving moving targets [26,27] where agreement between data and predictions were better for moving than for stationary targets. This is somewhat analogous to the present situation where this correspondence improves as the yaw angle increases [34]. Such a trend is partly due to the use here of a membrane theory which does not account for plug shear at normal incidence, but is indirectly accounted for in the application of the membrane equation which uses a striker velocity reduced from its initial value by the indentation process. The second reason for the superior agreement, when yaw is present, is that the tensile plate failure criterion must be supplemented by the requirement that the plug also has to be sheared, necessitating a higher striker velocity.

Table 2 also lists the percentage in the increase of the ballistic limit, Z, for the current experimental results of series 1 and 2 on aluminum, the theoretical value, and the data of [20].† In general, the predicted value of Z is larger than the experimental result, as was also found in the analogous case of moving targets. Finally, this table contains the data for the two series on 4130 steel; here, the wide divergence between the two test sequences is primarily attributed to a totally different heat treatment of the targets, as evidenced by their different yield and ultimate strengths. The effect of any similar difference in the strength and hardness properties of the two series of aluminum targets would be substantially less in view of their significantly lower magnitudes. The results are in accord with the observations of Grabarek [35] who estimated that the minimum velocity required for a projectile to perforate a plate at yaw angles up to 3° would need to be increased by no more than 1%.

† The authors are indebted to a reviewer for pointing out that a difference of about 10% in the unadjusted ballistic limit of Series 1 and 2 of the steel targets, as observed, is to be expected, based on minimum striker perforation energy and the difference in the ultimate strength of the two materials.

Table 2. Ballistic limits of targets

Comparison of data from Series 1 and Series 2, 2024-0 Al

Yaw angle α *(deg)*	*Experimental ballistic limit, Ser. 1* v_{50} *(m/s)*	*Experimental ballistic limit, Ser. 2* v_{50_0} *(m/s)*	*Adjusted ballistic limit, Ser. 2* v_{50a} *(m/s)*†	*% Difference,* $(v_{50}-v_{50a})/v_{50}$
0	153	133	148	3.3
5	156	139	154	1.3
10	159	143	159	0
15	165	146	162	1.8
19		185		

† v_{50a} is the ballistic limit for the second series adjusted for the mass difference in projectile/sabot mass between the two series, $v_{50a}=v_{50_0}$ (5.0/4.5).

Comparison of theoretical and experimental values, 2024-0 *Al*

Yaw angle α *(deg)*	*Experimental ballistic limit, Ser. 1* v_{50} *(m/s)*	*Theoretical ballistic limit,* v_{50th} *(m/s)* *(a)* S=200 *MPa*	*(b)* S=250 *MPa*	*% Difference* $(v_{50}-v_{50th})/v_{50}$ *(a)*	*(b)*
0	153	131	146	14.4	4.6
5	156	138	154	11.5	1.3
10	159	144	160	9.4	−0.6
15	165	150	166	9.1	−0.6

Percent increase in ballistic limit with yaw
$Z=100\times(v_{50}\langle\alpha^\circ\rangle-v_{50}\langle 0^\circ\rangle)/v_{50}\langle 0^\circ\rangle$

Yaw angle α *(deg)*	*Series* 1	2	*Theory*	*Ref.* [35]
5	2.0	4.5	5.3	3
10	3.9	7.5	9.2	12
15	7.8	9.8	13.7	–
19		12.6		

Experimental value of the ballistic limit for 4130 *Steel (m/s)*

Yaw angle α *(deg)*	*Series* 1	*Series* 2 v_{50_0}	*Adjusted Series* 2 v_{50a}
0	170	148	164
5		200	222
10	175	230	256
15		259	288
19		288	365

(c) *Other features*

The theoretical model will predict the final velocity of the projectile in cases of perforation only if the actual impact velocity is scaled to the value of the ballistic limit for the particular yaw angle employed. A typical example for a yaw of 15° is shown in Fig. 16. While agreement with the analysis is good near v_{50} in spite of some scatter due to experimental errors and the difficulty in precisely defining the ballistic limit, the divergence increases with initial impact velocity. The largest ratio of terminal to initial velocity was found both analytically and experimentally to occur at 5° yaw.

The final trajectory angle could not be measured when the projectile axis was not located in the plane perpendicular to the field of vision. As shown in Fig. 17, the prediction indicates

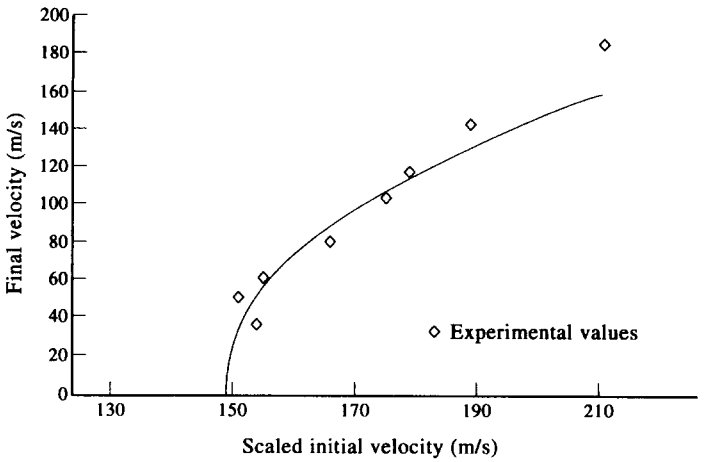

Fig. 16. Final vs initial velocity for aluminum, Series 1, at $\alpha = 15^{\circ}$

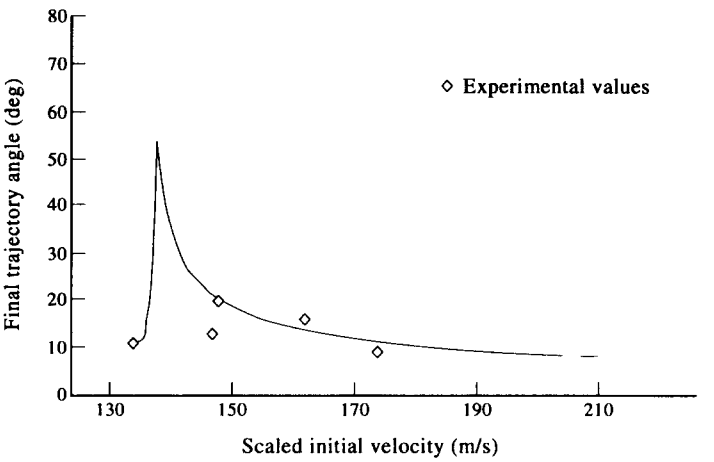

Fig. 17. Final trajectory angle, β, vs initial velocity for $\alpha = 5^{\circ}$.

a rapid rise of this parameter with impact speed near the ballistic limit, followed by an exponential decay. The difficulty of experimentally substantiating this spike is severe; while the data agrees with predictions away from the spike, missing information near this peak prevents a complete validation of the model. However, in view of the approximations incorporated in the representation of the event, the correspondence evident in this diagram as well as correlations involving the ballistic limit are considered to be satisfactory.

The present investigation represents the only analysis of yaw impact for projectiles (rather than rods) known to the authors. However, a number of models for oblique impact, which has many similar features, have been proposed. The relations of Ref. [7] for the final velocity of the striker have been compared with present experimental results. It was found that the predicted values are, with but one exception, uniformly lower by 12–30 per cent than the present measured exit speeds. This discrepancy can also be considered satisfactory for the reason cited above, although mechanistic differences may well be present between the two types of impact compared here.

CONCLUSIONS

An experimental investigation of the impact of 3.175 mm blunt, hard-steel strikers with an L/D ratio of 3 against 3.175 mm thick soft aluminum and hard steel target plates was performed. Initial velocities ranged from somewhat below to well above the ballistic limit

at yaw angles up to 19°. Target damage consisted of plug formation, bulging, and lateral indentation. Side petaling was found only for yaw angles of 10° or higher, while front petaling occurred only for 15° and 19°.

An analysis using some features from a moving target impact model was applied which depicted the process by consecutive stages of (a) initial indentation, considered to take place at normal incidence, (b) plate motion and failure as though occurring for normal impact concurrent with initial projectile rotation, (c) further projectile rotation during plug ejection, and (d) petaling damage produced by contact with the lateral projectile surface. The model underpredicted the experimental ballistic limit within $12 \pm 2\%$; this discrepancy was minimized in similar comparisons of other parameters upon multiplication of the measured initial velocity by the ratio of the experimental to the theoretical ballistic limit. For perforation runs, this yielded good correlation between data and predictions for the final velocity and fair agreement for the trajectory angle. The ballistic limit increased with increasing yaw angle, much more so for the stronger than for the weaker metallic target.

Acknowledgements—A portion of this work was sponsored by the Air Firce Office of Scientific Research under Contract No. AFOSR F49620-89-C-8127 and another portion by the U.S. Army Research Office under Contract DAAG29-80-K-0052 and by a gift from the FMC Corporation. A part of the work reported constituted a segment of a thesis by the second author submitted in partial fulfilment of the requirements of the M.S. degree at the University of California, Berkeley.

REFERENCES

1. A. C. Eringen (Editor), Penetration mechanics. *Int. J. Engng Sci.* **16** (11) (1978).
2. M. E. Backman and W. Goldsmith, The mechanics of penetration of projectiles into plates. *Int. J. Engng Sci.* **16**, 1–99 (1978).
3. T. W. Wright and K. Frank, Approaches to penetration problems. *SMIRT Symposium, No. 14, Impact.* Lausanne, Switzerland (1987).
4. C. E. Anderson and S. R. Bodner, The status of ballistic impact modelling. *Int. J. Impact Engng* **7**, 9–35 (1988).
5. R. F. Recht, High velocity impact dynamics: analytical modeling and plate penetration dynamics. In *High Velocity Impact Dynamics*, pp. 443–513 (Edited by J. A. Zukas *et al.*). J. Wiley, New York (1990).
6. W. Johnson, A. K. Segupta and S. K. Ghosh, High velocity oblique impact and ricochet mainly of long rod projectiles: an overview. *Int. J. Mech. Sci.* **24**, 425–434 (1982).
7. R. Recht and T. W. Ipson, Ballistic perforation dynamics. *J. Appl. Mech.* **60**, 384–390 (1963).
8. J. Awerbuch and S. R. Bodner, An investigation of oblique perforation of metallic plates by projectiles. *Exp. Mech.* **17**, 147–153 (1977).
9. R. L. Woodward and N. J. Baldwin, Oblique perforation of targets by small armor-piercing projectiles. *Int. J. Mech. Sci.* **21**, 85–91 (1979).
10. S. P. Virostek, J. Dual and W. Goldsmith, Direct force measurement in normal and oblique impact of plates by projectiles. *Int. J. Impact Engng* **6**, 247–269 (1987).
11. J. G. Hetherington and P. F. Lemieux, The effect of obliquity on the ballistic performance of two component composite armor. *Int. J. Impact Engng* **15**, 131–137 (1994).
12. M. E. Backman and W. Goldsmith, Penetration mechanics study. In *Recent Advances in Engineering Science. Proc. 14th Annual Meeting of the Society of Engineering Science*, pp. 3–8 (Edited by G. C. Sih). University of Lehigh Publications (1977).
13. M.E. Backman, S. A. Finnegan and K. C. Witham, Dynamics of the oblique impact and ricochet of nondeforming projectiles into thin plates. In *Recent Advances in Engineering Science. Proc. 14th Annual Meeting of the Society of Engineering Science*, pp. 9–20 (Edited by G. C. Sih). University of Lehigh Publications (1977).
14. I. M. Hutchings, The ricochet of spheres and cylinders from the surface of water. *Int. J. Mech. Sci.* **18**, 243–247 (1976).
15. M. Finnis, L. W. Longdon and G. M. Moss, The ricochet of spinning projectiles off water. *Proc. of the 12th Int. Symp. on Ballistics*, Vol. 3 (1990).
16. S. J. Bless, J. P. Barber, R. S. Bertke and H. F. Swift, Penetration mechanics of yawed rods. *Int. J. Engng Sci.* **16**, 829–834 (1978).
17. S. J. Bless and J. P. Barber, Bending waves in yawed rod impacts. *J. Ballistics* **2**, 281–298 (1978).
18. V. Hoehler and A. J. Stilp, The influence of primary yaw angle on the secondary yaw angle during armor plate perforation. *Proc. 6th Int. Symp. on Ballistics*, pp. 302–308 (1981).
19. M. Mayseless *et al.*, Bending waves in yawed rod impacts. *Proc. 6th Int. Symp. on Ballistics*, pp. 309–314 (1981).
20. J. E. Reaugh, *Penetration of Yawed Projectiles.* Univ. of California, Lawrence Livermore National Laboratory, Rept. UCRL-ID104890 (1990).

21. D. J. Cagliostro *et al.*, MESA 3-D calculations of armor penetration for projectiles with combined obliquity and yaw. *Int. J. Impact Engng* **10**, 81–92 (1990).
22. E. J. Hunter, *A Comparison of the CTH Shock Physics Code with Experimental Data.* Sandia Report 92-1899 (1992).
23. G. R. Johnson and W. H. Cook, Lagrangian code computations for oblique yawed rod impacts onto thin plates and spaced plate targets at various velocities. *Int. J. Impact Engng* **14**, 373–383 (1993).
24. A. J. Piekutowski and C. E. Anderson, Post-perforation characteristics of yawed long rods. *Proc. 14th Int. Symp. on Ballistics,* Vol. 2, pp. 527–536 (1993).
25. D. Yaziv, Z. Rosenberg and J. P. Riegel, Penetration capability of yawed long rod penetrator. *Proc. 14th Int. Symp. on Ballistics,* Vol. 2, pp. 202–207 (1993).
26. E. Wu and W. Goldsmith, Normal impact of blunt projectiles on moving targets: experimental study. *Int. J. Impact Engng* **9**, 389–404 (1990).
27. E. Wu and W. Goldsmith, Normal impact of blunt projectiles on moving targets: analytical considerations. *Int. J. Impact Engng* **9**, 405–432 (1990).
28. A. Prakash, Supercomputer simulations of impact of cylindrical projectiles on moving plates. *Proc. 1991 Summer Computer Simulation Conference* (23rd), pp. 543–547 (1991).
29. O. Ruiz and W. Goldsmith, Controlled tumbling of projectiles—I. Theoretical model; II. Experimental results. *Int. J. Impact Engng* **7**, 101–115, 285–305 (1988).
30. M. A. Persechino and A. E. Williams, Tumbling of hypervelocity rods induced by impact with oblique plate targets. *Int. J. Impact Engng* **14**, 561–571 (1993).
31. J. Liss, W. Goldsmith and F. E. Hauser, Constraint to side flow in plates. *J. Appl. Mech.* **50**, 694–698 (1983).
32. P. Beynet and R. Plunkett, Plate impact and plastic deformation by projectiles. *Exp. Mech.* **11**, 64–70 (1971).
33. J. Liss, W. Goldsmith and J. M. Kelly, A phenomenological penetration model of the penetration of thin plates. *Int. J. Impact Engng* **1**, 321–341 (1983).
34. Eric Tam, *Yaw Impact on Plates by Blunt-nosed Projectiles.* Thesis (M.S.) Univ. of California, Berkeley (1991).
35. C. Grabarek, (Aberdeen Proving Grounds), Personal communication.